minerals

Article

Geochemistry and Petrogenesis of the Wadhrai Granite Stock of the Malani Igneous Suite in Nagar Parkar Area, SE Pakistan

M. Qasim Jan [1,*], M. Hassan Agheem [2], Tahseenullah Khan [3], Hafiz U. Rehman [4,*] and Akhtar Hussain Markhand [2]

1 National Centre of Excellence in Geology, University of Peshawar, Peshawar 25130, Pakistan
2 Centre for Pure & Applied Geology, University of Sindh, Jamshoro 76080, Pakistan
3 Department of Earth and Environmental Sciences, Bahria University, Islamabad 44000, Pakistan
4 Graduate School of Science and Engineering, Kagoshima University, Kagoshima 890-0065, Japan
* Correspondence: mqjan@yahoo.com (M.Q.J.); hafiz@sci.kagoshima-u.ac.jp (H.U.R.)

Abstract: The Wadhrai granite stock is a part of the Nagar Parkar Igneous Complex, an extension of the Neoproterozoic Malani Igneous Suite of western Rajasthan. It is occupied by a petrographically uniform granite comprising perthite, plagioclase, quartz, with small quantities of biotite, opaque oxides, titanite, and secondary minerals. The rocks are sparingly porphyritic and contain dykes of microgranite, aplite, and rare pegmatite. In the south-central part, parallel sheets and swarms of mafic dykes, and in the western part very fine-grained felsic sheets intrude the body. The granite is metaluminous to peraluminous and characterized by high silica (73–76 wt%), and alkalis (7–9 wt%), and low CaO (0.15–1.4 wt%), MgO (0.15–0.38 wt%), Th (7–12 ppm), and U (1–2 ppm). On geochemical discriminant diagrams, it classifies mostly as A-type (with rather high Y/Nb (8.6 to 2.4, average 5.2) and low Nb/Ga and Ce (typical of A2-type), but sparingly as I-type. Chondrite-normalized patterns show enrichment in LREE over HREE, and small negative Eu anomalies, whereas mantle-normalized spidergrams display higher LILE over HFSE, distinct troughs for Nb, Sr, P, Ti, and spikes for La, Ce, Nd, Sm and Tb. The granite magma was possibly derived from a tonalite-granodiorite-dominated crustal source. Based on the above-mentioned geochemical evidence, it is interpreted that the source rocks of the magma of the Wadhrai granite likely developed initially in a continental margin subduction setting and underwent partial melting in a continental extensional environment.

Keywords: Wadhrai granite; Nagar Parkar igneous complex; Malani igneous suite; SE Pakistan; geochemistry; petrogenesis

check for updates

Citation: Jan, M.Q.; Agheem, M.H.; Khan, T.; Rehman, H.U.; Markhand, A.H. Geochemistry and Petrogenesis of the Wadhrai Granite Stock of the Malani Igneous Suite in Nagar Parkar Area, SE Pakistan. *Minerals* **2022**, *12*, 1240. https://doi.org/10.3390/min12101240

Academic Editors: Jaroslav Dostal and Alexey V. Ivanov

Received: 23 August 2022
Accepted: 26 September 2022
Published: 30 September 2022

1. Introduction

The Nagar Parkar area of SE Sindh covers 500 km^2 along the Great Rann of Kutch and the Thar Desert in Pakistan. It comprises mounds and hills of granites in a plain covered by sand, silt and salt. The granites are emplaced in a suite of metamorphosed mafic to felsic rocks and are cut by younger mafic and felsic dykes, collectively referred to as the Nagar Parkar Igneous Complex (NPIC). The granites consist of grey (Karunjhar-type, with aegirine and riebeckite), and whitish grey to pink varieties (containing biotite ± hornblende) [1–3]. A simplified geological map of the area is shown in Figure 1. Petrographic similarities, radiometric ages, and geographic proximity suggest that the NPIC belongs to the Malani Igneous Suite (MIS) of western Rajasthan [4]. It is considered as the third largest felsic igneous province in the world [5], and the largest of its type in India [6]. Bimodal magmatism and associated clastic sediments occur in the Punagarh and Sindreth basins (24°50′ N, 72°47′ E) located along the eastern margin of the Malani rocks [6]. The MIS is Neoproterozoic in age; 700–800 Ma [4,7–10]. U–Th–Pb zircon ages on the main granites of NPIC are similar to these, with a few older dates like those of Erinpura [3,11–13]. Comprehensive age data [14] show that the Neoproterozoic granitic magmatism in the NPIC spanned >100 Ma from ca. 775

to 640 Ma. Rehman et al. [15] also reported 272 ± 5.4 Ma felsic dykes in the area, possibly associated with Permian rifting of the Cimmerian microcontinents from the Gondwana.

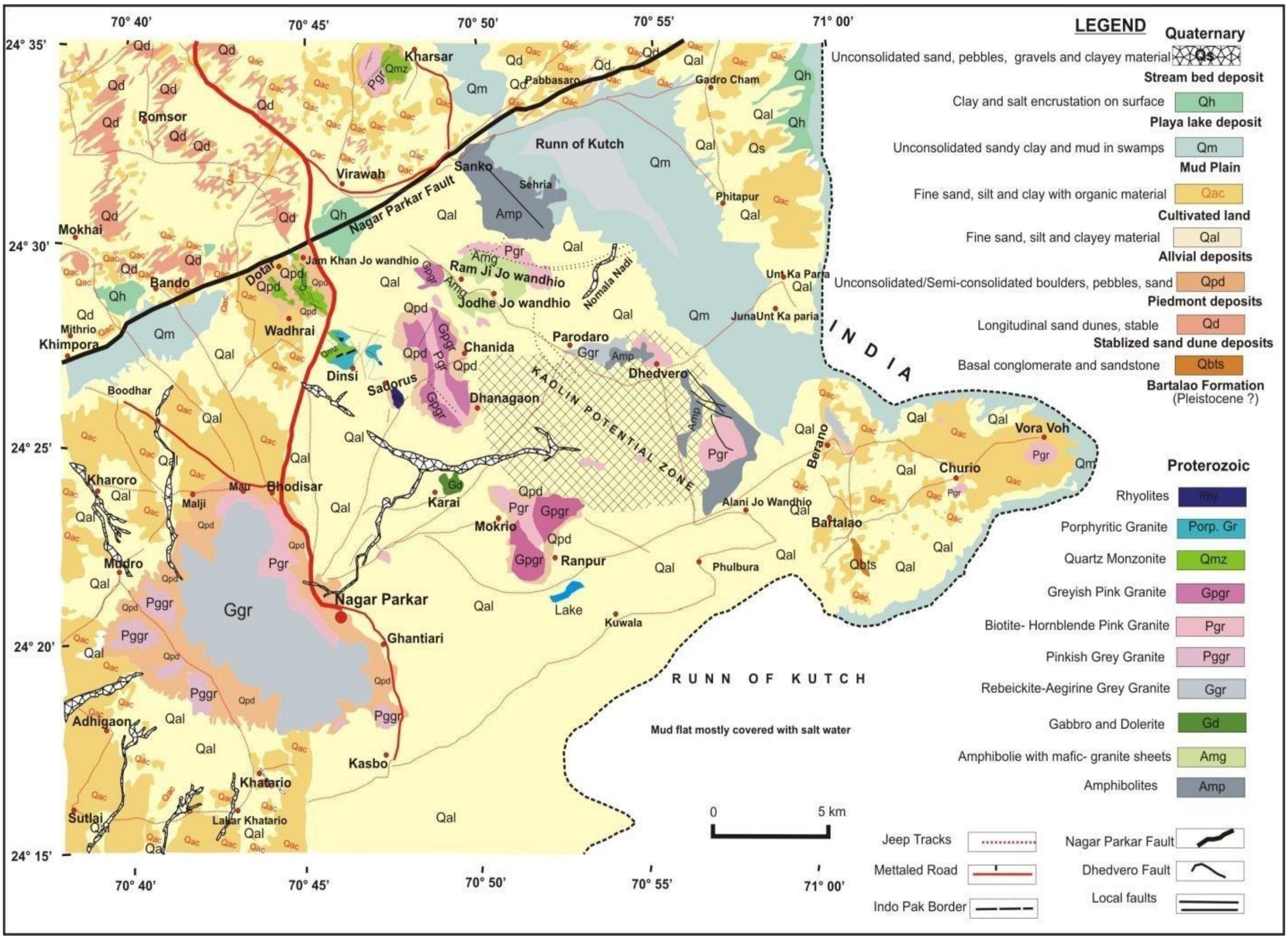

Figure 1. Simplified geological map of the Nagar Parkar igneous complex, SE Pakistan (modified after [16].

This paper deals with the geochemistry and petrology of the Wadhrai stock, exposed 12 km north of the Nagar Parkar town (28°28′22″ N, 70°45′40″ E, Figure 1). Covering > 10 km^2, it is essentially composed of granite that contains many mafic and felsic dykes (Figure 2).

The Wadhrai stock has been previously investigated in some detail; however, not much attention has been paid to its petrogenesis and magmatic evolution. Jan et al. [16] mapped the stock and provided petrographic details. Markhand et al. [12] briefly described the geochemistry of various rocks of the body, and reported a U-Pb zircon age of 767 ± 12 Ma on the main Wadhrai granite. While discussing the geochemistry of the NPAC, Ref. [2] provided major and trace element analyses of six samples from Wadhrai. However, detailed petrology and petrogenesis have not been reported on the Wadhrai granite itself. The aim of this study was to present analytical results of major and trace element data to trace the petrological evolution of the Wadhrai granite and the tectonic environment that prevailed during its magma generation.

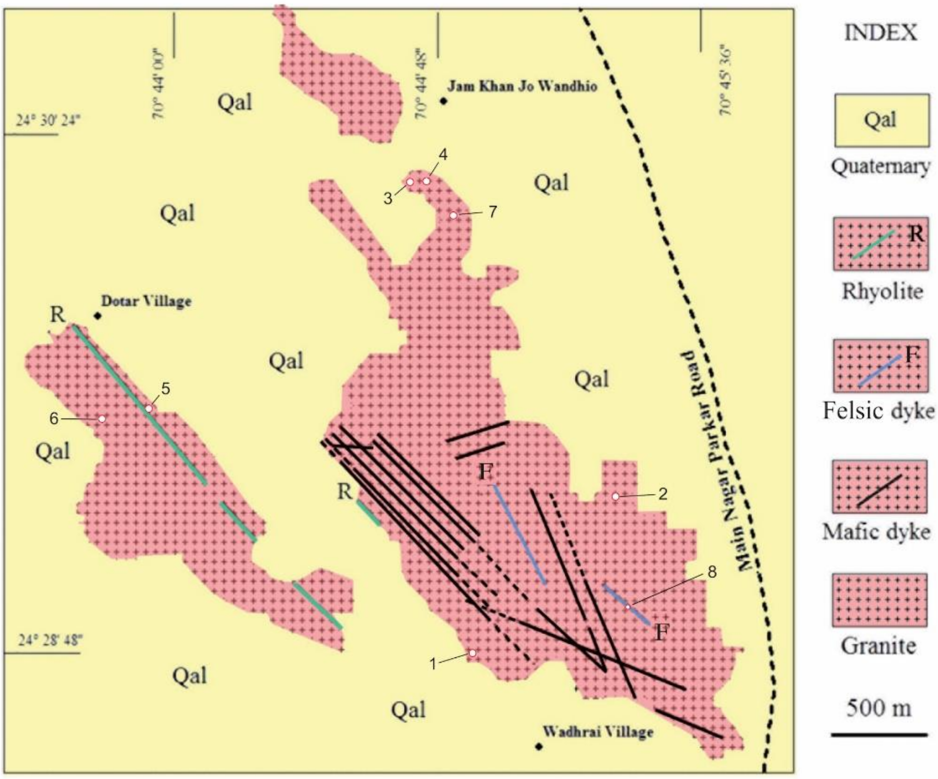

Figure 2. Geological map of the Wadhrai granite stock (modified after [16]. Numbers show the location of the analyzed samples.

2. Petrography

The Wadhrai stock is made up of spheriodally weathered, uniform granite of light color, locally showing pinkish hue (Figure 3A,B). It is cut by mafic and felsic dykes (Figure 3C–E), which are particularly abundant in the southern part (Figure 2). It contains sparse mafic enclaves of the basement, and greyish granitic autoliths. The granite displays medium- to fine-grained granitic texture, and is sparingly porphyritic with >1 cm long feldspar phenocrysts. The granite is composed of perthite, plagioclase (both mildly cloudy), quartz, small amounts of biotite, chlorite (after biotite), opaque oxides, titanite, leucoxene (secondary), and rare allanite and epidote (Figure 3F). The plagioclase is commonly zoned, at places oscillatory, and ranges from sodic andesine to albite. Details on petrography are reported in [16].

The felsic dykes comprise microgranite, aplite and, rarely pegmatite (Figure 3C,D). Most of the dykes do not exceed 150 m in length and 2 m in thickness; some are vein-like (Figure 3D) and less than 10 m in length. They are locally cut by mafic dykes, or the two may sparingly form composite sheets. The dykes are fine-grained, subequigranular to subporphyritic, and hypidiomorphic. They essentially consist of feldspar and quartz, small quantities of opaque oxides, with or without biotite, amphibole, titanite, rare epidote and secondary minerals. Details on petrography can be found in [1].

There also are a few very fine-grained felsic dykes, one of which extends 2 km in length. These dykes are marginally banded, and locally display conchoidal fractures (Figure 3E). They are sparsely porphyritic and show granophyric and spherulitic fabric. They consist of perthite, albite, quartz, sodic amphibole, sodic clinopyroxene, and small quantities of opaque oxides, titanite, allanite, and rare epidote, tourmaline and olivine. Details on petrography can be found in [1]. The presence of sodic amphibole and sodic clinopyroxene suggests that the rocks are sodic and peralkaline.

Figure 3. Field and petrographic aspects of the Wadhrai granite. (**A**) Spheroidal weathering in granite. (**B**) Pink color in the weathered granite is further accentuated by the evening sun. (**C**) Fresh granite intruded by thin mafic dykes, hammer for scale. (**D**) Felsic dyke (50 cm wide) in jointed and weathered granite. (**E**) Grey fine-grained felsic dyke (right) in weathered granite (left), hammer for scale. (**F**) Photomicrograph of a typical granite from east central part of the body, composed of perthite (Prt), zoned plagioclase (Pl) showing some alteration, quartz (Qtz), partly chloritized biotite (Bt), chlorite (Chl) and opaque grains. Length of the photograph is 2.5 mm.

Mafic dykes range from layers to 10–15 m thick and >1 km long bodies (Figure 2), often in parallel sets separated by meters to tens of meters of the host granite in the south central part of the granite body. The dykes show considerable variation in modal composition and texture from distinctly porphyritic to aphyric, medium-grained to (mostly) fine-grained, and fresh to altered. Some of the dykes possess many fractures, are highly weathered, and locally turned brown to chocolate color. In the less altered rocks, phenocrysts of labradorite (<5 mm to (rarely) 3 cm) and local amphibole and clinopyroxene lie in a groundmass comprising plagioclase (calcic andesine to sodic labradorite), clinopyroxene or brown primary amphibole, biotite, and ilmenite. The altered rocks contain saussuritized plagioclase, secondary amphibole, chlorite, biotite, ilmenite, with or without titanite/leucoxene, calcite, quartz, chalcedony and rare serpentine.

3. Geochemistry

In this paper, we present geochemical data of granite samples collected from the Wadhrai body for a closer look into its petrogenesis and the tectonic environment in which it originated. Eight representative samples of the granite (analyses #1–8 in Table 1) were analyzed for major (expressed in wt%) and trace elements (in ppm) using X-ray fluorescence (XRF), and rare-earth elements (REE, also in ppm) were analyzed using the inductively coupled plasma mass spectrometer (ICP-MS). Before the analyses, the selected samples were mechanically crushed to a powder of 200 mesh size, and decomposed with lithium tetraborate flux. Fused glass beads were used for major and trace element analysis using XRF. Loss on ignition (LOI) was performed at 1000 °C on fractions of the powdered samples. For REE analysis, sample powders were decomposed using the HF-HNO_3-$HClO_4$ acid digestion method and the solutions were measured by ICM-MS. The detection limits of XRF for major elements was 0.01% and those of ICP-MS were 0.01 to 1 ppm, respectively. For instrumental calibration geological standard reference materials from USGS and GSJ were used. In addition, six samples from the Wadhrai body, published in an earlier study [2], were also reproduced in Table 1 (analyses #9–14) for comparison.

3.1. Major Element Data

Whole-rock major data of the studied samples (Table 1) are characterized by high SiO_2 (73–76 wt%), and eight of the analyses contain normative corundum (Table 2). Total alkalis range from 7.3 to 9.2 wt%, and K_2O/Na_2O ratios range from 0.6 to 1.1 (with one value of 1.8). Normative color index (wt% mafic minerals) ranges from 2.6 to 4.5 (average 3.8) and 100 An/(An + Ab) ranges from 3.5 to 14.7 (average 10.4; ignoring analysis #5 with no normative An). Al_2O_3, TiO_2, total FeO, MgO, CaO and Na_2O show negative correlation, while K_2O show positive correlation with SiO_2. A positive correlation of Ti with MgO was also observed. Previous authors (e.g., [2,12,17]) classified the rocks as adamellite. However, major element chemistry does not support this nomenclature. On the normative An–Ab–Or diagram (Figure 4A) of O'Connor [18] and on the R1 (4Si − 11(Na + K) − 2(Fe + Ti)) vs. R2 (6Ca + 2(Mg + Al)) diagram (Figure 4B) of De La Roche et al. [19], the analyzed samples plot in a granite field. For measure of alkalinity, the data were plotted on the SiO_2 vs (Al_2O_3 + CaO + Na_2O + K_2O)/(Al_2O_3 + CaO + Na_2O − K_2O) diagram of Middlemost [20] (Figure 4C) where all the 14 analyses classify as alkaline.

Table 1. Whole rock major (wt%), trace and rare-earth element (ppm) data of the Wadhrai granite.

Sample	1	2	3	4	5	6	7	8	9	10	11	12	13	14
SiO_2	75.2	75.5	73.86	73.55	76.13	73.44	73.44	73.26	76.25	75.05	74.38	74.75	76.87	76.29
TiO_2	0.3	0.27	0.33	0.33	0.23	0.29	0.26	0.28	0.26	0.27	0.32	0.29	0.16	0.22
Al_2O_3	12.78	12.32	13.86	14.12	11.16	13.38	13.71	13.26	12.96	13.92	13.59	14.11	13.12	13.04
Fe_2O_3	1.14	1.97	2.09	2.09	2.64	1.95	1.72	1.75	0.74	0.84	0.92	0.87	0.61	0.7
FeO									0.81	0.92	1.02	0.96	0.68	0.77
MnO	0.08	0.08	0.07	0.08	0.1	0.06	0.07	0.09	0.03	0.07	0.07	0.08	0.04	0.08
MgO	0.32	0.32	0.35	0.38	0.15	0.33	0.28	0.23	0.36	0.35	0.28	0.35	0.17	0.39
CaO	0.89	0.36	1	1.09	0.15	0.91	0.96	1.4	0.99	1.06	1.21	0.99	0.44	1.09
Na_2O	5.02	4.92	4.23	4.41	4.64	4.89	4.96	4.72	2.66	3.75	4.83	3.9	3.82	3.53
K_2O	3.45	3.19	3.83	3.6	4.53	3.58	3.77	2.89	4.68	3.73	3.34	3.66	4.09	3.86
P_2O_5	0.03	0.04	0.04	0.04	0.02	0.05	0.05	0.06	0.24	0.03	0.04	0.03	0.01	0.04
LOI	0.8	0.88	0.33	0.39	0.62	0.7	1.02	1.97						
Total	100	99.85	99.99	100.1	100.4	99.58	100.2	99.91	99.98	99.99	100	99.99	100	100
Ba	644		726	797	20	730	770	440	454	684	661	705	796	879
Zr	63		344	294	1340	771	732	309	160	249	292	269	189	110
Rb	41.6		88	81	96.4	88	93.3	76	146	111	69	95	87	101
Th	11.5		8	8	12	7.2	9.7	8.7	12	14	15	10	13	7
Ta	1.1				1.1	0.7	1	0.9	4	6	4	7	5	7

Table 1. *Cont.*

Sample	1	2	3	4	5	6	7	8	9	10	11	12	13	14
Nb	6.2		14	11	15.8	10.3	11.5	11.9	15	13	12	14	10	10
Hf	3.5				28.6	17.9	18.2	8.6	6	8	8	8	8	9
Y	53.6		50	42	106	76.2	81.3	54.7	50	47	45	50	37	24
Sr	72		99	119	108	101.5	104.5	76.7	90	96	111	100	29	135
Ga			22	21					19	20	20	20	20	16
Cs					0.63	1.39	1.92	1.14	3.5	1.82	2.66	2.66	3.12	2.98
Sc									4	6	7	3	4	3
U					1.8	1.6	2.2	1.8	2.74	3.44	1.21	2.24	2.56	3.52
La	38.1				36.4	27.5	34.1	32.3	45.34	39.78	35.44	34.55	36.66	33.24
Ce	70.8		110	100	110.5	65.4	77.9	74.9	113.1	102.5	76.66	99.89	96.13	88.12
Pr	9.2				12.45	7.87	9.09	8.61	11.98	14.78	12.34	12.55	12.33	11.13
Nd	42.9		52	41	50.2	34.6	37.7	35.2	27.34	30.75	44.34	30.34	32.56	21.35
Sm	8.4				11	7.86	7.79	7.39	6.91	7.67	13.45	15.15	13.12	12.54
Eu	1.4				1.97	1.47	1.38	1.4	1.18	1.57	1.28	1.34	1.18	1.65
Gd	8.2				10.15	7.87	7.93	7.52	9.67	10.12	10.15	9.55	9.05	10.12
Tb	1.3				1.97	1.33	1.37	1.3	1.77	1.54	1.35	1.34	1.07	1.37
Dy	8.4				12.85	8.46	8.8	8.34	10.14	11.22	9.22	11.09	11.12	9.77
Ho	1.8				2.72	1.74	1.8	1.78						
Er	5.5				8.52	5.18	5.77	5.6	3.17	3.73	0.62	6.25	6.38	5.66
Tm					1.32	0.84	0.93	0.9						
Yb	5.7				8.9	5.59	6.28	6.18	6.78	6.79	5.65	5.34	6.88	6.56
Lu					1.36	0.85	0.97	0.92	0.93	1.14	1.21	1.23	1.14	1.15

Table 2. CIPW Norms calculated from the major oxides of the studied granitic samples.

Sample	1	2	3	4	5	6	7	8	9	10	11	12	13	14
Q	30.78	32.98	31.24	30.51	33.61	28.49	27.36	31.46	40.17	35.39	29.72	34.61	37.16	37.43
C	0	0.21	1.03	1.08	0	0	0	0	2.29	1.85	0	2	1.63	1.16
or	20.57	19.08	22.75	21.38	26.89	21.43	22.48	17.46	27.67	22.05	19.75	21.64	24.18	22.82
ab	42.85	42.13	35.97	37.49	32.31	41.49	42.36	40.84	22.52	31.75	40.89	33.02	32.33	29.88
an	2.15	1.54	4.72	5.17	0	4.02	4.03	6.59	3.35	5.07	5.53	4.72	2.12	5.15
di	1.75	0	0	0	0.54	0.19	0.38	0.1	0	0	0.19	0	0	0
hy	0.9	2.92	2.99	3.08	3.53	2.76	2.3	2.38	2.51	2.81	2.68	2.88	1.9	2.63
Mt	0.34	0.51	0.55	0.55	0	1.28	1.22	1.28	0.42	0.48	0.53	0.5	0.34	0.41
il	0.57	0.52	0.63	0.63	0.44	0.56	0.5	0.54	0.49	0.51	0.61	0.55	0.3	0.42
ap	0.07	0.09	0.09	0.09	0.04	0.11	0.11	0.13	0.52	0.07	0.09	0.07	0.02	0.09
CI	3.56	3.95	4.17	4.26	4.51	4.01	3.63	3.49	3.43	3.8	4.01	3.93	2.55	3.45
An mol%	4.8	3.5	11.6	12.1	0	8.8	8.7	13.9	12.9	13.8	11.9	12.5	6.2	14.7

On Shand's [21] molecular Al/(Na + K) vs. Al/(Ca + Na + K) diagram (Figure 4D), the analyses show a range from metaluminous to mildly peraluminous. For comparison, we also show fields of A-type granitoids from (1) NW Junggar region of the Central Asian Orogenic Belt in NW China [22], (2) Hassanrobat, Iran [23], and (3) Khalifan, Iran [24]. It is interesting to note that the Wadhrai analyses show a spread like the A-type granitoids of Junggar, but eight of the analyses plot in the overlapping fields of the two A-type granitoids from Iran. The A/CNK value of 1.1 is considered to divide I-type and S-type granites [21]. A/CNK in Wadhrai ranges from 0.81 to 1.16, but in ten of the analyses it is <1.1, suggesting the possibility of an I-type rather than S-type protolith for the granite.

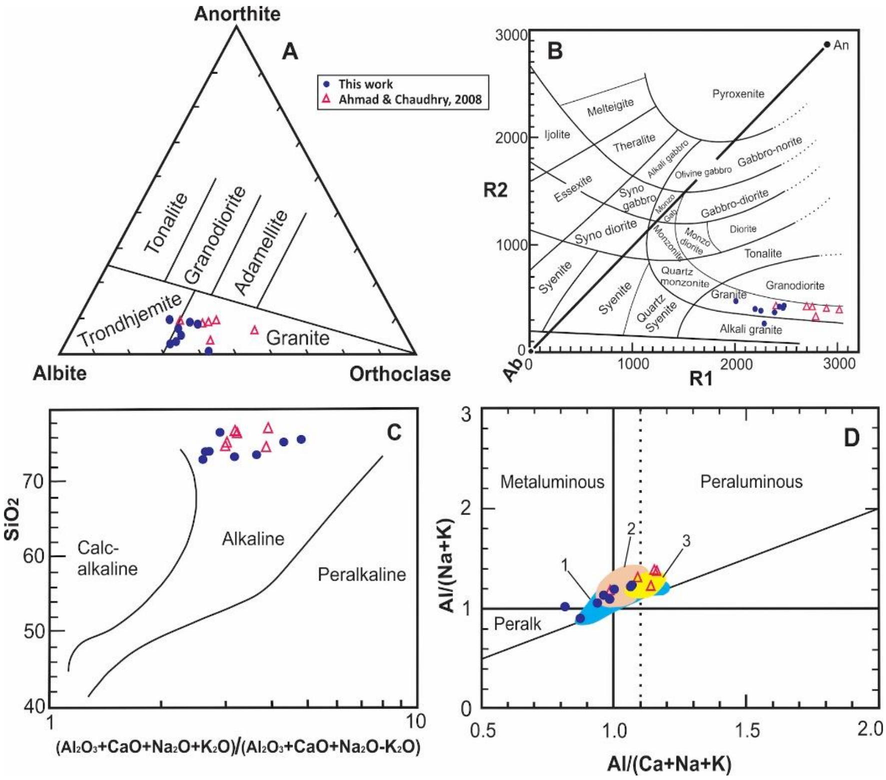

Figure 4. Classification of Wadhrai granite according to different chemical schemes. (**A**) Normative anorthite–albite–orthoclase classification [18]. (**B**) R1 (4Si − 11(Na + K) − 2(Fe + Ti)) vs. R2 (6Ca + 2(Mg + Al)) classification scheme of De La Roche et al. [19]. (**C**) SiO_2 vs. (Al_2O_3 + CaO + Na_2O + K_2O)/(Al_2O_3 + CaO + Na_2O − K_2O) relations classification diagram after [20]. (**D**) Molecular Al/(Na + K) vs. Al/(Ca + Na + K) diagram after [21]. Dashed line separates granites of igneous source (left) from granites derived from sediments (right). Fields for A-type granites are for comparison: 1—Junggar (Siluro-Devonian) granite, Central Asian orogenic belt, NW China [22], 2—Hasanrobat Permian granite, Sanandaj-Sirjan belt, Iran [23], 3—KhalifanVariscan granite, NW Iran [24].

A series of other proposed procedures were used to decipher the A-type, I-type and S-type nature of the Wadhrai granite. On the K_2O versus Na_2O diagram [25], the analyses plot in the field of I-type granites (Figure 5A). On the FeO*/(FeO* + MgO) diagram of [26], the analyses plot in the A-type field (Figure 5B).

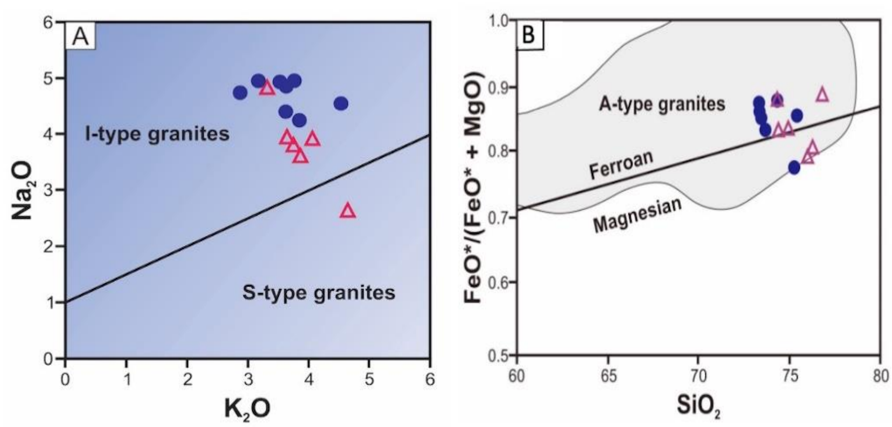

Figure 5. Discrimination diagrams of granites. (**A**) Na_2O vs. K_2O diagram discriminating I-type and S-type granitic rocks (after [25]). (**B**) FeO*/(FeO* + MgO) vs. SiO_2 discrimination diagram displaying the fields for ferroan and magnesian granites. A-type granites plot in the shaded area (after [26]). Symbols as in Figure 4.

3.2. Trace and Rare-Earth Element Data

Trace and rare-earth elements (REE) concentrations of the analyzed samples are shown in Table 1. To decipher petrogenesis of the Wadhrai granite, a number of commonly used discrimination diagrams for granitoids are used. On Zr versus 10,000 Ga/Al (Figure 6A) and Nb versus 10,000 Ga/Al (Figure 6B) diagrams of Whalen et al. [27], the Wadhrai analyses plot in A-type granite field in both these diagrams. On (Na_2O + K_2O)/CaO and FeOt/MgO vs. Zr + Nb + Ce + Y diagrams [27], the analyses straddle the A-type and unfractionated M-, I- and S-type granites (figure not shown). The A-type granites have been subdivided on the basis of Nb–Y–3Ga and Nb–Y–Ce contents into two types [28,29], one of which (A_1) is characterized by element ratios similar to oceanic island basalts, and the other (A_2) incorporates analyses of granitic rocks derived from continental crust or underplated crust which has gone through continent-continent collision or island arc magmatism. In both these diagrams (Figure 7A,B), the Wadhrai data plot in A_2 field, which is supported by the rather high Y/Nb (2.5–8.6, average 4.8) and Yb/Ta (1.0–8.1, average 3.5) ratios of the analyses. The Ce/Nb versus Y/Nb plot (Figure 7B) of the analyses is compared with rocks from different tectonic environments reported in [28,29].

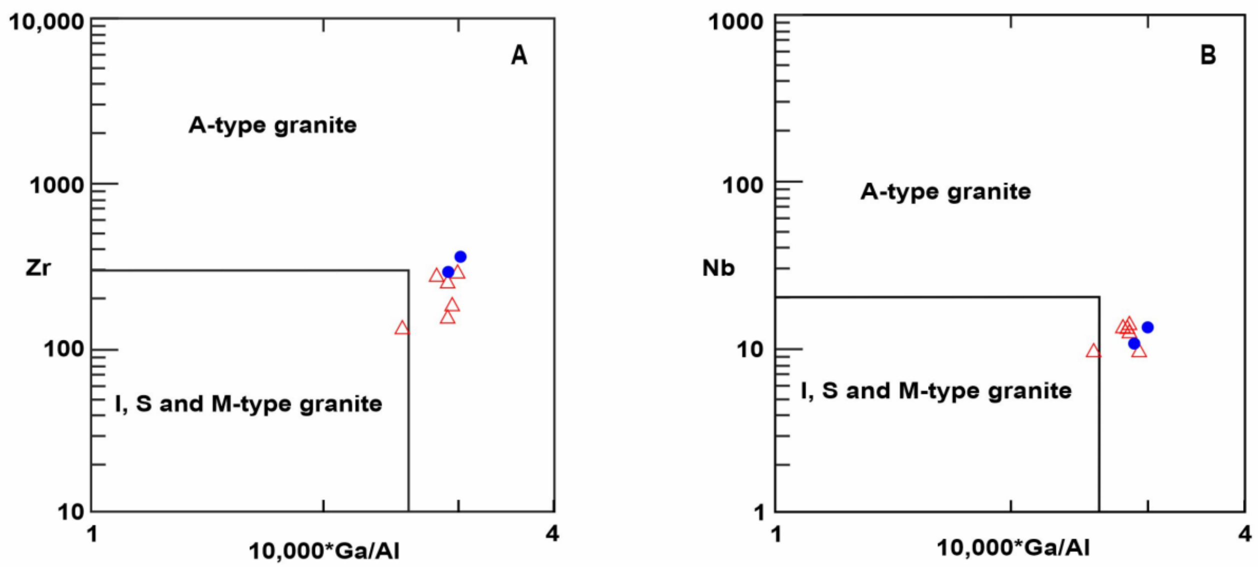

Figure 6. Discrimination diagrams of granites. (**A**) Zr versus 10,000 Ga/Al and (**B**) Nb versus 10,000 Ga/Al diagrams of Whalen et al. [27] in which the Wadhrai analyses plot in the A-type granite field in both these diagrams.

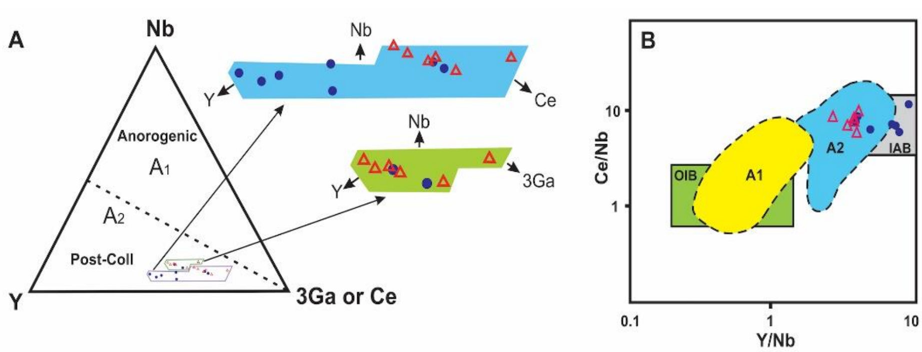

Figure 7. Plots of Wadhrai analyses on granitoid discrimination diagrams. (**A**) Nb–Y–3Ga and Nb–Y–Ce ternary diagrams [28] used for distinguishing A_1 and A_2 sub-type granitoids. (**B**) Ce/Nb vs. Y/Nb relations, showing fields of oceanic island basalt (OIB), A_1 and A_2-type granites and island arc basalt (IAB) [28,29]. Our data mainly plot in the A_2-type granite field. Symbols as in Figure 4.

Plots of the analyses on the rather widely used discrimination diagrams [30] are displayed in Figure 8, with fields for post-collision granites (PCG) after [31] in A and [32] in B. In Rb vs. Y + Nb (Figure 8A) and Nb vs. Y (Figure 8B) diagrams, the analyses straddle the adjacent fields of volcanic arc granites (VAG) and within plate granites (WPG). However, they are confined to the fields of post-collision A-type granites.

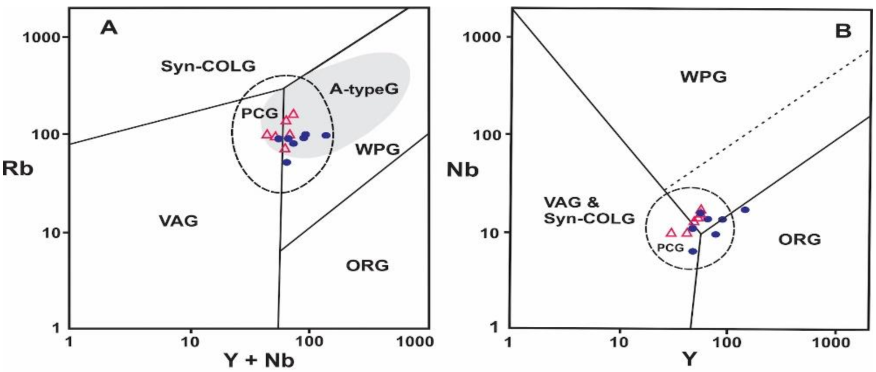

Figure 8. Plot of the Wadhrai granite analyses on Rb vs. Y+Nb (**A**) and Nb vs. Y (**B**) diagrams after [30], showing fields of Syn-collisional- (Syn-COLG), Within plate- (WPG), Ocean ridge- (ORG), and Volcanic arc (VAG) granites. Field for post-orogenic/post-collision granites (PCG) is after [31] in (**A**) and after [32] in (**B**). The A-type shaded area in A is after [27]. The dashed line in B marks the upper compositional limit for ORG from anomalous ridge segments. Symbols as in Figure 4.

The normalized trace- and rare-earth elements plots for the Wadhrai samples are shown in Figure 9. The chondrite-normalized REE patterns of the Wadhrai analyses are compared with those of the Mt. Abu pluton of the MIS (shaded area shown in Figure 9A) in Rajasthan reported by [9]. A close match in the two is obvious; both show an increase in the LREE over the HREE and a negative Eu anomaly that is distinct in the Mt. Abu. The patterns and Eu anomaly are also similar to those of the Sindreth rhyolite to the north of Mt. Abu [6]. The depletion in Eu may reflect source characteristic, retention of plagioclase or fractionation of plagioclase. Using values from Wood et al. [33], primordial mantle normalized spidergram for a range of trace elements is shown in Figure 9B. There are higher quantities of the normalized large ion lithophile elements (LILE) than high field strength elements (HFSE), resulting in an overall slope towards the right (less incompatible elements). More significantly, there are distinct troughs for Nb, Sr, P, and Ti, and spikes for La, Ce, Nd, Sm, and Tb. These features, particularly the negative Nb anomaly, are characteristic of subduction-related magmas.

In order to explore further the origin of Wadhrai granite, selected trace elements were compared with other rocks of similar aspects. Figure 9C shows a comparison with Mt. Abu A-type granite (shaded area) for which arc origin has been argued strongly by [9]. Normalized trace-element patterns in rocks of the MIS ca. Jaswantpura peraluminous volcanics reported by [34] and Jalor granite reported by [35], and granitoids of Seychelles ca. Praslin group presented by [36,37] were shown by [9] in their Figure 7. The results from the above-mentioned localities are more or less identical to those of Wadhrai. However, despite the close similarity in patterns, the Wadhrai granite has lower values for most of the LILE (except Ba and similar K). For Mt. Abu, Ashwal et al. [9] explained the prominent depletions in Ba, Sr and Eu in terms of source retention of plagioclase, since no evidence for fractional crystallization was noted. The normalized trace-elements patterns of the Wadhrai granite are also similar (except for a lack of distinct negative Ba anomaly) to those of the Mibaishan granite (Sulu orogen, China) which has been considered as derived from subducted continental crust [38].

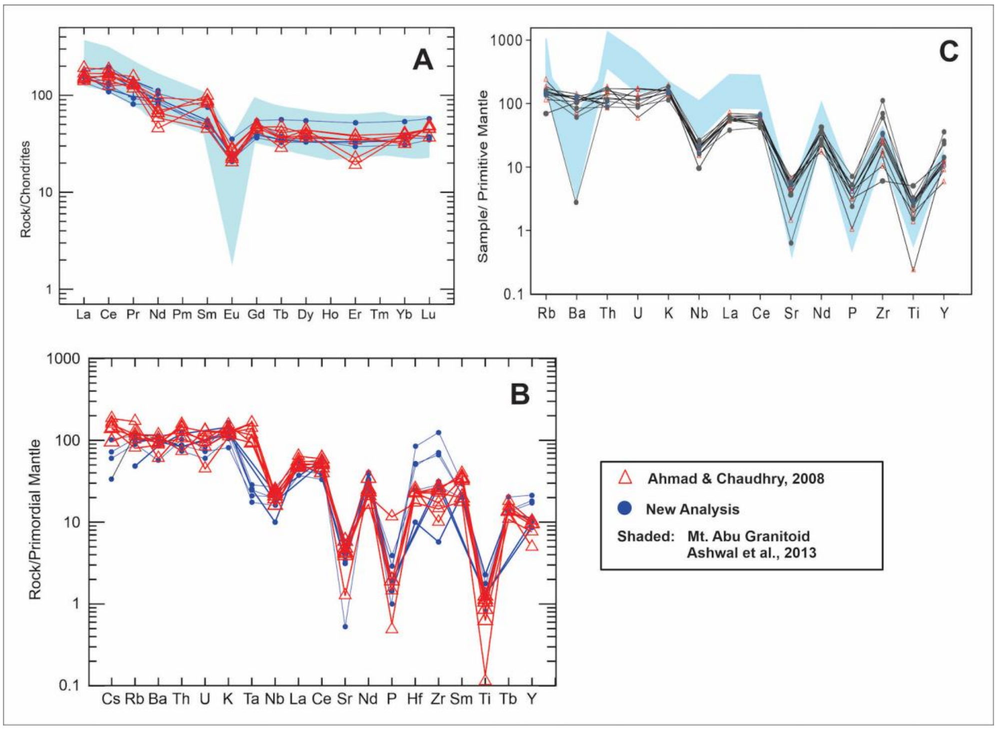

Figure 9. (**A**) Chondrite-normalized REE contents of the Wadhrai granite. Normalizing values are after [39]. (**B**) Primordial mantle normalized spidergram for a wide range of trace elements in the Wadhrai granite. Normalizing values are after [32]. (**C**) Selected trace elements normalized to primordial mantle of [40]. Superposed shaded pattern in A and C is the field of analyses from Mt. Abu granitoid of the MIS in Rajasthan after [9]. The patterns of the analyses from Mt. Abu and Wadhrai are remarkably similar except for Ba, Th and U.

4. Discussion

Petrographic comparison, proximity and sporadic exposures in the intervening areas between major bodies in MIS and Nagar Parkar led previous researchers to suggest that the NPIC is an extension of the MIS (e.g., [1–3,10,13]). Butt et al. [41] tentatively correlated the NPIC with the Mt. Abu granite. Laghari [17] suggested pink granites of the NPIC are equivalent to those of Jalor granites in Rajasthan, and the grey granites to those of the Erinpura body. Based on the above inferences, the Wadhrai granite provides important insights to understand its petrogenesis on local scale and its role in the tectonic scenario of the MIS on regional scale. Below, we discuss details on petrogenesis, timings of the magmatism in NPIC and MIS, and the tectonic settings.

4.1. Petrogenetic and Geochronological Implications

The Wadhrai body shares rock-types and petrographic features with the other main granite bodies of the NPIC and MIS [42,43]. It is principally made up of light-grey, biotite leucogranite that was likely produced mainly from the within-plate magmatism but the source of the magma may have been generated form the subduction-related protolith. In addition, three distinct types of dykes (mafic, well-crystallized felsic, and fine-grained felsic dykes) intrude the granite. At least some of the well-crystallized felsic dykes (microgranite, aplite, and rare pegmatite) can be related to the host granite. No cross-cutting relations have been observed between the mafic and fine-grained felsic dykes, but they may be a product of late bimodal magmatism as proposed for the Kharsar hillock in northern Nagar Parkar [42]. Bimodal magmatism has been reported from MIS and several other areas of the world [44]. Underplating of the crust by mafic magma can result in partial melting of the crust and production of felsic magma, and this has been proposed as one of the viable mechanisms for bimodal mafic-felsic magmatism, as in Death Valley, California [45]. Kochhar et al. [46]

suggested ponding of the crust by basaltic magma, coupled with extensional tectonics, for bimodal magmatism in Jalor area of Rajasthan.

Radiometric age-data further support the correlation of the two. Khan et al. [3] reported U–Th–Pb zircon and monazite ages of 900–1100 Ma on grey granites and 700–800 Ma on pink granites of the NPIC. The Wadhrai main granite and pink granite yielded ages of 767 $\pm$ 12 Ma and 803 $\pm$ 7.8 Ma, respectively [12]. These dates are mostly congruous with those of the MIS [43], and others in references. In a detailed study, Rehman et al. [14] showed that the NPIC granites formed over a period of 775 to 640 Ma, with a peak around 750 Ma, and their data confirm the opinion that the NPIC is a part of the Malani Large Igneous Province. Another recent study by Rehman et al. [47], based on zircon U–Pb coupled with in-situ Hf isotope data, proposed a tectonic model that showed the initiation of magmatism due to the oceanic subduction of the Mozambique Ocean along the western periphery of the Rodinia Supercontinent, and the peak magmatism was reached during the rifting afterwards. The Whadrai granite likely retains geochemical signatures from both the subduction-associated early-stage and rift-related late-stage magmatism. The existing U–Pb zircon age data, ca. 750 Ma, on Wadhrai granite [3,12,14] provide clear evidence for the rift-related late-stage magmatism, also consistent with results obtained from MIS, Seychelles, Madagascar, and South China (for details see [47] and references therein). However, no older ages have been found yet from the Wadhrai body. Further works are needed to make a clear distinction for the above two types of tectonic settings.

To support our interpretations stated above, and to decipher the tectonic settings of the Wadhrai granite, a number of geochemical discrimination diagrams have been used. The discrimination diagrams display chemical characteristics of the I-type granites (Figure 5A) that can be further sub-categorized into A-type granitoids (Figures 5B and 6A,B). According to [28], the A_2-type granitoids represent rocks belonging to different tectonic locales, including those derived from continental crust or underplated crust that has gone through continent-continent collision or island-arc magmatism. The Wadhrai granite shares features of post-collision/within plate granites on (Rb vs. Y + Nb and Nb vs. Y (Figure 8A,B). Mantle-normalized multi-trace element spidergram exhibited by enrichment in LILE and depletion in HFSE, and distinct spikes and troughs, are typical of subduction-related rocks. Their REE and trace element patterns (Figure 9A,B) are very similar to those of the A-type Mt. Abu granite [9], Sindreth-Punagarh volcanics [36], and Seychelles Praslin group granitoids, all of which have been considered to have formed in a continental margin arc. However, the Wadhrai granite has much lower Th and U contents and Th/U ratios when compared with Mt. Abu and other A-type granites, and in this regard is similar to I-type rocks [48].

4.2. Origin and Proposed Tectonic Setting

A variety of tectonic models have been proposed for the MIS granitoids (including the NPIC, the Mt. Abu granite, and the volcanics of Sindhreth-Punagarh basins), and equivalents in Seychelles, northern Madagascar and elsewhere [10]. Most of these models center around the fundamental question of whether the felsic magmatism in the MIS developed (i) in a continental extensional environment through melting of the crust, with or without necessitating the additional role of a mantle plume or hotspot [4,10,41–43,46,49–51], or (ii) in a subduction-related (continental) arc environment [9,36,52,53]. The volcano-sedimentary association comprising 761–769 Ma basalt, rhyolitic tuffs and associated clastic sediments of the Sindreth and Punagarh basins along the eastern margin of the MIS to the north of Mt. Abu has been traditionally considered to be related to continental rift. Schobel et al. [54] argued strongly in favor of such an origin for the Sindreth basin. However, Ref. [36] suggested a continental arc origin for the rhyolitic tuffs from Sindreth. Detailed geochemical data, according to [6], are "consistent with magma derived from continental crust that has been through a cycle of continent-continent collision or an island-arc setting". A localized extension within an overall convergent scenario" was proposed for the volcanics of the Sindreth and Punagarh basins. Kochhar [55] showed a widespread distribution of the Neoproterozoic Malani type magmatism in the Middle East, South China, Tarim, Mongolia and Siberia in support of large-scale rifting during the Neoproterozoic.

On the basis of geochemistry, the tectonic locale of the Wadhrai granite can be interpreted in more than one way, and there is no compelling evidence to stick to the widely held opinion that the NPIC is continental rift-related. The Nagar Parkar granitoids were correlated by [3] with the 750 Ma Seychelles granitoids which, according to [52], developed in Andean-type continental margin. Khan et al. [3] also suggested that the NPIC granitoids generated from the partial melting of island arc crust in a rift-related, within-plate setting. A more or less similar suggestion was made by [6] for the derivation of Punagarh volcanics magma. Khan et al. [3] also inferred that "being part of Trans-Aravalli Belt of the Indian shield, the Nagar Parker area . . . shouldered the Seychelles islands towards the western side of Rodinia before the supercontinent rifted in Neoproterozoic" (see also Figure 1 of Gregory et al. [8], and Figure 8 of Rehman et al. [47]).

Jan et al. [56] have shown that the Nagar Parkar granitoids are emplaced in a calc-alkaline basement comprising mafic rocks, tonalite, and granite developed in an Andean-type continental margin. Red granite of the basement near Dhedvero, which shows high degree of brittle deformation, has a U-Pb-Th date of 830 Ma [17], which has been considered as the minimum age for the Nagar Parkar basement. Hence, in agreement with [17] and [56], the Wadhrai and other NPIC granites were not only emplaced in a basement consanguineous with the 860–880 Ma Erinpura [57] basement, but possibly were also derived from it. Modal mineralogy, notably the presence of biotite and titanite, and rock chemistry showing $Na_2O > 3.2$ wt% and molar Al/(Ca + Na + K) < 1.1 has been considered as characteristic of I-type granites [26,58]. On the ACF diagram (Figure 10A), the Wadhrai granite, plotting in I-type field, supports its derivation from crustal meta-igneous rocks. The possible derivation of the Wadhrai granite from a tonalitic-granodioritic source is suggested by the plots on the 3CaO–($5K_2O/Na_2O$)–Al_2O_3/(FeOt + MgO) (Figure 10B, [59]). It is, therefore, suggested that the Wadhrai granite magma was mainly derived from a crustal source of island arc origin dominated by tonalite-granodiorite composition. In summary, it is likely that the Wadhrai granite (like others in NPIC) was derived through anataxis of continental crust which was generated in subduction-related continental margin during its earlier stages and evolved into the rift-related tectonic setting afterwards.

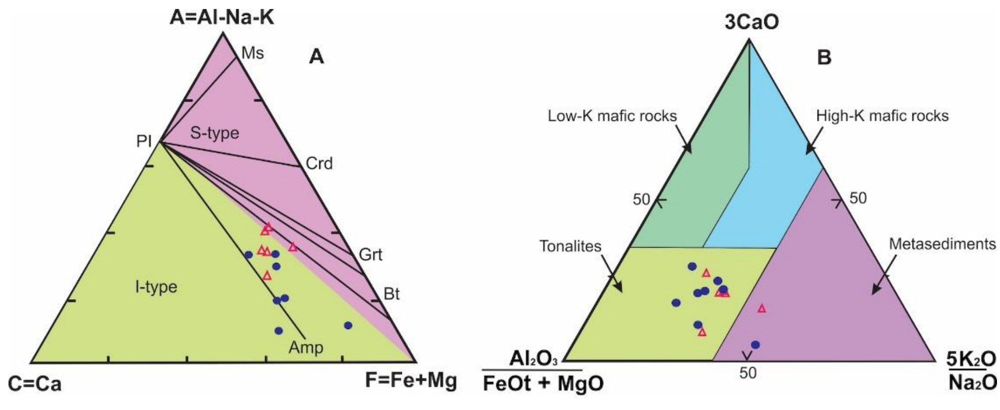

Figure 10. (**A**) Plots of the Wadhrai granite analyses on (**A**) mole% ACF diagram, showing the fields for S- and I-type granitoids [26]. (**B**) 3CaO–($5K_2O/Na_2O$)–Al_2O_3/(FeOt + MgO) diagram showing fields representing the composition of melts derived from a range of potential sources [59]. Symbols as in Figure 4.

4.3. Crystallization Temperature of Granites and Inferred Pressure Conditions

Operating pressures for the rocks were estimated using a normative quartz–albite–orthoclase diagram showing experimentally calibrated isobars after [60], and Rb–Sr diagram with pressure contours after [61]. Positions of the analyses in Figure 11A suggest pressures of 4 to 6 kbar (13–20 km depth), and in Figure 11B 25 to 27 km depth. We consider that the higher values represent the depth of magma formation in the lower part of middle crust/upper part of lower crust, and the lower values show depth of magma crystallization. The average La/Yb content (5.6) of the analyses is closer to that (5.3) of the lower crust than that (10.9) of the middle crust [62].

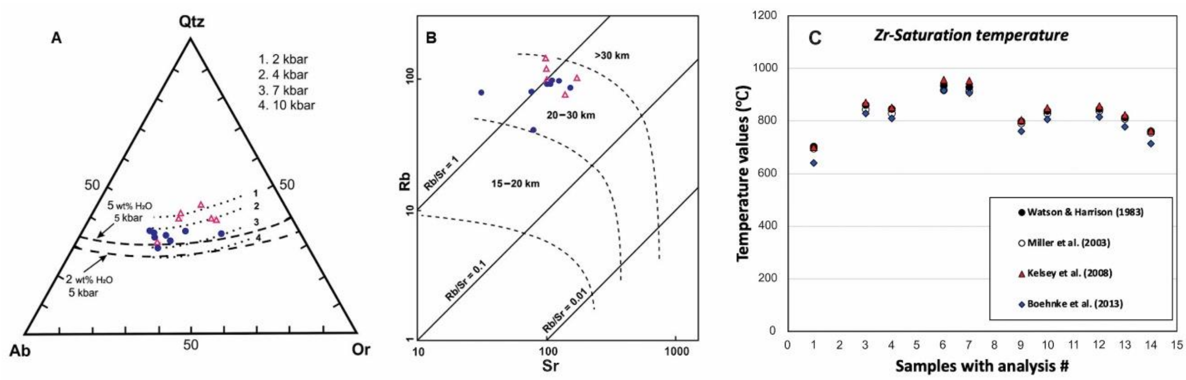

Figure 11. Plots of Wadhrai analyses for estimation of pressure and temperature conditions for the Wadhrai granitic rocks. (**A**) Normative Quartz–Albite–Orthoclase diagram showing experimentally calibrated isobars after [59,63]. (**B**) Rb against Sr plots and pressure relations after [61]. (**C**) Zircon saturation temperature estimates, calculated after the procedures reported in [62–65].

Zircon saturation temperatures (Table 3, Figure 11C), varying between 770 and 870 °C, were obtained from the Wadharai granites using the procedures of [64–67]. These estimates are similar to those (784 to 918 °C) obtained for Nagar Parkar pink and grey granites [47], and likely represent operating temperatures during magma generation.

Table 3. Zircon saturation temperatures from the analyzed samples of Wadhrai granite.

Sample	1	3	4	5	6	7	9	10	12	13	14	Average
Watson & Harrison (1983) [64]	703	861	845	987	935	928	799	838	846	814	762	847
Kelsey et al. (2008) [65]	700	870	852	1015	958	953	805	849	858	824	764	859
Boehnke et al. (2013) [66]	641	830	811	973	915	907	761	806	816	778	715	814
Miller et al. (2003) [67]	695	844	829	960	916	913	791	830	837	809	755	834

* Foot note: Analysis #2, 8 and 11 were discarded due to erroneous Zr contents and unrealistic temperature values.

The moderate negative Eu anomaly in chondrite normalized pattern of the REE in the Wadhrai granite (Figure 10A) was attributed to source characteristic, retention of plagioclase at the site of melting or fractionation of plagioclase. The Sc/Th vs. SiO_2/Al_2O_3 relations (Figure 12A, after [68]) suggest minor biotite fractionation, just as Rb/Sr vs. Sc relations (Figure 12B, after [68]) support a small degree of feldspar fractionation.

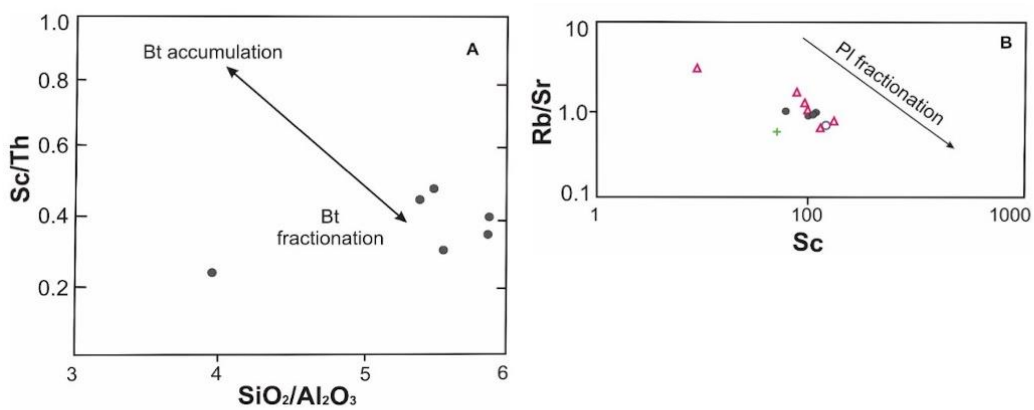

Figure 12. (**A**) Sc/Th vs. SiO_2/Al_2O_3 relations showing the biotite fractionation and accumulation trends, adopted from [68], and (**B**) Rb/Sr vs. Sr relations showing feldspar fractionation, after [68].

5. Conclusions

1. The Wadhrai granite stock of the NPIC is an extension of the Malani Igneous Suite.
2. It is made up of a uniform hypersolvus, biotite-granite characterized by high silica, Fe#, and alkalis.
3. The granite analyses classify it as I-type, and specifically as A-type, on various geochemical discrimination diagrams.
4. The magma was developed in continental extensional environment from source material that possibly developed in a subduction-related setup, but the possibility cannot be entirely ruled out that that the granite magma may have belonged to a continental margin subduction regime.
5. The granite magma was likely derived from a tonalite-granodiorite-dominated crustal source, generated initially in a subduction-related continental margin and evolved into the rift-related tectonic setting.
6. The magma was possibly generated at a depth of about 25–27 km and at 770–870 °C, and crystallized at 19–13 km depth.
7. It underwent a small degree of feldspar and biotite fractionation.

Author Contributions: Field work, M.Q.J., M.H.A. and T.K.; petrography: M.Q.J. and M.H.A.; conceptualization: M.Q.J. and H.U.R.; chemical analyses: T.K. and A.H.M.; writing and review: M.Q.J. and H.U.R., with suggestions from M.H.A., T.K. and A.H.M. All authors have read and agreed to the published version of the manuscript.

Funding: This research was partly funded by the Pakistan Academy of Sciences through grant No. PAS R.G. 103.

Data Availability Statement: Not applicable.

Acknowledgments: M.Q.J. wishes to thank the Pakistan Academy of Sciences for a research grant for geological studies in the Nagar Parkar area. Sarfaraz H. Solangi and the Director of the Centre for Pure & Applied Geology, University of Sindh, Jamshoro, kindly provided logistical support. Ikram Abbasi, Abuzar Ghaffari, Khalid Latif and M. Zeeshan are acknowledged for preparation of the figures. We are thankful for the constructive comments provided by five reviewers that improved the contents and illustrations significantly.

Conflicts of Interest: There is no conflict of interest.

References

1. Jan, M.Q.; Laghari, A.; Khan, M.A. Petrography of the Nagar Parkar igneous complex. Tharparkar, Southeastern Sindh, Pakistan. *Geol. Bull. Univ. Peshawar* **1997**, *30*, 227–259.
2. Ahmad, S.A.; Chaudhry, M.N. A-type granites from the Nagarparkar complex, Pakistan: Geochemistry and origin. *Geol. Bull. Punjab Univ.* **2008**, *43*, 69–81.
3. Khan, T.; Murata, M.; Rehman, H.U.; Zafar, M.; Ozawa, H. Nagarparker granites showing Rodinia remnants in the southeastern part of Pakistan. *J. Asian Earth Sci.* **2012**, *59*, 39–51. [CrossRef]
4. Bhushan, S.K. Malani rhyolite—A review. *Gondwana Res.* **2000**, *3*, 65–77.
5. Pareek, H.S. Petrochemistry and petrogenesis of the Malani Igneous Suite, India. *Geol. Soc. Am. Bull.* **1981**, *92*, 206–273.
6. Wang, W.; Pandit, M.K.; Zhao, J.; Chen, W.; Zheng, J. Slab break-off triggered lithosphere asthenosphere interaction at a convergent margin: The Neoproterozoic bimodal magmatism in NW India. *Lithos* **2017**, *296–299*, 281–296. [CrossRef]
7. Kochhar, N. Geological evolution of the Trans-Aravalli block (TAB) of the NW Indian Shield and Seychelles connection in the Late Proterozoic: Evidence from plume related A-type Malani magmatism. *Geol. Surv. India Spec. Publ.* **2004**, *84*, 247–264.
8. Gregory, L.C.; Meert, J.G.; Bingen, B.; Pandit, M.K.; Torsvik, T.H. Paleomagnetism and geochronology of the Malani Igneous Suite, Northwest India: Implications for the configuration of Rodinia and the assembly of Gondwana. *Precambrian Res.* **2009**, *170*, 13–26. [CrossRef]
9. Ashwall, L.D.; Solanki, A.M.; Pandit, M.K.; Corfu, F.; Hendriks, B.W.H.; Burke, K.; Torsvik, T.H. Geochronology and geochemistry of Neoproterozoic Mt. Abu granitoids, NW India: Regional correlation and implications for Rodinia paleogeography. *Precambrian Res.* **2013**, *236*, 265–286. [CrossRef]
10. de Wall, H.; Pandit, M.K.; Donhauser, I.; Schobel, S.; Wang, W.; Sharma, K.K. Evolution and tectonic setting of the Malani–Nagarparkar: A Neoproterozoic silicic-dominated large igneous province in NW India-SE Pakistan. *J. Asian Earth Sci.* **2018**, *160*, 136–158.

11. Khan, T.; Murata, M.; Jan, M.Q.; Rehman, H.U.; Zafar, M.; Ozawa, H.; Qadir, A.; Mehmood, S. Felsic dykes in the Neoproterozoic Nagar Parkar Igneous complex, SE Sindh, Pakistan: Geochemistry and tectonic settings. *Arab. J. Geosci.* **2017**, *10*, 308. [CrossRef]
12. Markhand, A.H.; Xia, Q.; Agheem, M.H.; Jia, L. U-Pb Zircon dating and geochemistry of the rocks at Wadhrai body, Nagar Parkar Igneous Complex, Sindh, Pakistan. *Sindh Univ. Res. J. Sci. Ser.* **2017**, *49*, 1–6.
13. Mastoi, A.S.; Yang, X.; Deng, J.; Hakro, A.A.A.D. Early Neoproterozoic evolution of southeast Pakistan: Evidence from geochemistry, geochronology, and isotopic composition of the Nagarparkar igneous complex. *Int. Geol. Rev.* **2019**, *61*, 1391–1408.
14. Rehman, H.U.; Khan, T.; Jan, M.Q.; Lee, H.-Y.; Chung, S.-L.; Murata, M. Timing and span of the continental crustal growth in SE Pakistan: Evidence from LA-ICP-MS U-Pb zircon ages from granites of the Nagar Parkar Igneous Complex. *Gondwana Res.* **2018**, *61*, 172–186. [CrossRef]
15. Rehman, H.U.; Khan, T.; Lee, H.-Y.; Chung, S.-L.; Murata, M.; Jan, M.Q. Permian felsic magmatism in the Neoproterozoic Nagar Parkar Igneous Complex of the Malani Igneous Suite: Evidence from zircon U–Pb age. *Isl. Arc* **2019**, *28*, e12323. [CrossRef]
16. Jan, M.Q.; Agheem, M.H.; Laghari, A.; Anjum, S. Geology and petrography of the Nagar Parker igneous complex, southeastern Sindh: The Wadhrai body. *J. Himal. Earth Sci.* **2016**, *49*, 1–13.
17. Laghari, A. Petrology of the Nagar Parkar Granites and Associated Basic Rocks, Thar District, Sindh, Pakistan. Ph.D. Thesis, University of Peshawar, Peshawar, Pakistan, 2004.
18. O'Connor, J.T. A classification for quartz-rich igneous rocks based on feldspar ratios. *US Geol. Surv. Prof. Pap.* **1965**, *525B*, B79–B84.
19. De la Roche, H.; Leterrier, J.; Grandle Claude, P.; Marchal, M. A classification of volcanic and plutonic rocks using R1–R2 diagrams and major element analyses- its relationships and current nomenclature. *Chem. Geol.* **1980**, *29*, 193–210. [CrossRef]
20. Middlemost, E.A.K. Naming materials in the magma igneous rock system. *Earth Sci. Rev.* **1994**, *37*, 215–224. [CrossRef]
21. Shand, S.J. *The Eruptive Rocks*, 2nd ed.; John Wiley: New York, NY, USA, 1943; p. 444.
22. Yin, J.; Chen, W.; Xiao, W.; Yuan, C.; Windley, B.F.; Yu, S.; Cai, K. Late Silurian-early Devonian adakitic granodiorite, A-type and I-type granites in NW Junggar, NW China: Partial melting of mafic lower crust and implications for slab roll-back. *Gondwana Res.* **2017**, *43*, 55–73. [CrossRef]
23. Alirezaei, S.; Hassanzadeh, J. Geochemistry and zircon geochronology of the Permian A-type Hasanrobat granite, Sanandaj-Sijan belt: A new record of the Gondwana break-up in Iran. *Lithos* **2012**, *151*, 1221–1234. [CrossRef]
24. Bea, F.; Mazhai, A.; Montero, P.; Amini, S.; Ghalamghash, J. Zircon dating, Sr and Nd isotopes, and element geochemistry of the Khalifan pluton, NW Iran: Evidence for Variscan magmatism in a supposedly Cimmerian super terrane. *J. Asian Earth Sci.* **2011**, *40*, 172–179. [CrossRef]
25. Chappell, B.W.; White, A.J.R. Two contrasting granite types: 25 years later. *Aust. J. Earth Sci.* **2001**, *48*, 489–499. [CrossRef]
26. Frost, B.R.; Barnes, C.G.; Collins, W.J.; Arculus, R.J.; Ellis, D.J.; Frost, C.D. A geochemical classification for granitic rocks. *J. Petrol.* **2001**, *42*, 2033–2048. [CrossRef]
27. Whalen, J.B.; Curry, K.L.; Chappell, B.W. A-type granites: Geochemical characteristics, discrimination and petrogenesis. *Contrib. Mineral. Petrol.* **1987**, *95*, 407–419. [CrossRef]
28. Eby, G.N. Chemical subdivision of A-type granitoids: Petrogenetic and tectonic implications. *Geology* **1992**, *20*, 641–644. [CrossRef]
29. Eby, G.N. The A-type granitoids: A review of their occurrence, and chemical characteristics and speculation on their petrogenesis. *Lithos* **1990**, *26*, 115–134. [CrossRef]
30. Pearce, J.A.; Harris, N.B.W.; Tindle, A.G. Trace element discrimination diagrams for the tectonic interpretation of granitic rocks. *J. Petrol.* **1984**, *25*, 956–983. [CrossRef]
31. Pearce, J.A. A user's guide to basalt discrimination diagrams: Trace element geochemistry of volcanic rocks: Applications for massive sulphide exploration. *Geol. Assoc. Can. Short Course Notes* **1996**, *12*, 79–113.
32. Danishvar, N.; Maanijou, M.; Azizi, H.; Asahaar, Y. Petrogenesis and geodynamic implications of an Ediacaran (550 Ma) granite complex (metagranites), southwestern Saqqez, northwest Iran. *J. Geodyn.* **2019**, *132*, 101669. [CrossRef]
33. Wood, D.A.; Joron, J.L.; Treuil, M. A reappraisal of the use of trace elements to classify and discriminate between magma series erupted in different tectonic settings. *Earth Planet. Sci. Lett.* **1979**, *45*, 326–336. [CrossRef]
34. Maheshvari, A.; Garhia, S.S.; Sial, A.N.; Ferreira, V.P.; Dwivedi, V.; Chittora, V.K. Geology and geochemistry of granites around Jaswantpura, Jalor district, southwestern Rajasthan, India. *Precambrian Res.* **2002**, *5*, 37–379.
35. Carter, L.M. Granitic and Rhyolitic Magmatism: Constraints on Continental Reconstruction from Geochemistry, Geochronology and Palaeomagnetism. Master's Thesis, Rand Afrikaan University, Johannesburg, South Africa, 2005; p. 54.
36. Ashwal, L.D.; Demaiffre, D.; Torsvik, T.H. Petrogenesis of Neoproterozoic granitoids and related rocks from Seychelles: The case of an Andean-type arc origin. *J. Petrol.* **2002**, *43*, 4–83. [CrossRef]
37. Dharma Rao, C.V.; Santosh, M.; Kim, S.W. Cryogenian volcanic arc in the NW Indian Shield: Zircon SHRIMP U-Pb geochronology of felsic tuffs and implications for Gondwana assembly. *Gondwana Res.* **2012**, *22*, 36–53.
38. Zhao, Z.F.; Zheng, Y.F.; Chen, Y.X.; Sun, G.C. Partial melting of subducted continental crust: Geochemical evidence syn-exhumation granite in Sulu orogeny. *Geol. Soc. Am. Bull.* **2017**, *129*, 1692–1707. [CrossRef]
39. Anders, E.; Grevesse, N. Abundances of the elements: Meteoritic and solar. *Geochim. Cosmochim. Acta* **1989**, *53*, 17–214. [CrossRef]
40. White, W. Geochemistry, Online Textbook. 2007, p. 413. Available online: http://www.geo.cornell.edu/geology/classes/geo455/Chapter.html (accessed on 7 November 2021).

41. Butt, K.A.; Jan, M.Q.; Karim, A. Late Proterozoic rocks of Nagar Parkar, southeastern Pakistan: A preliminary petrologic account. In *Geology in South Asia-1*; Ahmed, R., Sheikh, A.M., Eds.; Hydrocarbon Development Institute of Pakistan: Islamabad, Pakistan, 1994; pp. 106–109.
42. Jan, M.Q.; Agheem, M.H.; Laghari, A.; Anjum, S. Geology and petrography of the Nagar Parkar igneous complex, southeastern Sindh, Pakistan: The Kharsar body. *J. Geol. Soc. India* **2017**, *89*, 91–98. [CrossRef]
43. Sharma, K.K. Malani-magmatism: An extensional lithospheric tectonic origin. *Geol. Soc. Am. Spec. Pap.* **2005**, *388*, 463–476.
44. Winter, J.D. *An Introduction to Igneous and Metamorphic Petrology*; Prentice Hall: New York, NY, USA, 2010; p. 702.
45. Smith, E.I.; Tibbetts, A.; Belmontes, H.; Johnsen, R.; Walker, J.D. Pliocene basaltic and rhyolitic volcanism in the Greenwater Range, Death Valley area, California. In Proceedings of the Natural History Conference, Death Valley Natural History Association, San Diego, CA, USA, February 2016; pp. 3–43.
46. Kochhar, N.; Dhar, S.; Sharma, R. Geochemistry and tectonic significance of acid and basic dykes associated with Jalor magmatism, west Rajasthan. *Mem. Geol. Soc. India* **1995**, *33*, 375–389.
47. Rehman, H.U.; Khan, T.; Lee, H.-Y.; Chung, S.-L.; Jan, M.Q.; Zafar, T.; Murata, M. Petrogenetic source and tectonic evolution of the Neoproterozoic Nagar Parkar complex granitoids: Evidence from zircon Hf isotope and trace element geochemistry. *Precambrian Res.* **2021**, *354*, 106047. [CrossRef]
48. Regelous, A.; Scharfenberg, L.; De Wall, H. Origin of S-, A-, and I-type granites: Petrogenetic evidence from whole rock Th/U ratio variations. *Minerals* **2021**, *11*, 672. [CrossRef]
49. Kochhar, N. Malani Igneous Suite: Hot spot magmatism and cratonisation of the northern part of the Indian shield. *J. Geol. Soc. India* **1984**, *25*, 155–161.
50. Kochhar, N. A-type Malani magmatism, northwestern peninsular India. In *Glimpses of Geoscientific Research in India*; Singhvi, A.K., Bhattacharya, A., Guha, S., Eds.; Indian National Science Academy: New Delhi, India, 2008; pp. 176–181.
51. Srivastava, K.R.; Maheshwari, A.; Upadhyaya, A. Geochemistry of felsic volcanics from Gurapratap Singh and Diri, Pali district, Rajasthan (Part II, trace elements). *J. Geol. Soc. India* **1989**, *34*, 617–631.
52. Torsvick, T.H.; Ashwal, L.D.; Tucker, R.D.; Eide, D.A. Neoproterozoic geochronology of the Seychelles microcontinent: The India link. *Precambrian Res.* **2001**, *110*, 47–59. [CrossRef]
53. Solanki, A.M. A Petrographic, Geochemical and Geochronological Investigation of Deformed Granitoids from SW Rajasthan: Neoproterozoic Age of Formation and Evidence of Pan-African Imprint. Master's Thesis, University of the Witwatersrand, Johannesburg, South Africa, 2016; 216p.
54. Schobel1, S.; Sharma, K.K.; Horbrand, T.; Bohm, T.; Donhauser, I.; de Wall, H. Continental rift setting and evolution of Neoproterozoic Sindreth Basin in NW-India. *J. Earth Syst. Sci.* **2017**, *126*, 90. [CrossRef]
55. Kochhar, N. The Greater Malani Supercontinent: South China, Siberia, Mongolia, Kazakhstan, and Tarim connection during the Neoproterozoic. In *Precambrian Evolution and Deep Exploration of the Continental Lithosphere*; IAGR Conference Series: Beijing, China, 2013; pp. 51–57.
56. Jan, M.Q.; Laghari, A.; Khan, M.A.; Agheem, M.H.; Khan, T. Petrology of calc-alkaline/adakitic basement hosting A-type Neoproterozoic granites of the Malani Igneous Suite in Nagar Parkar, SE Sindh, Pakistan. *Arab. J. Geosci.* **2018**, *11*, 25. [CrossRef]
57. de Wall, H.; Regelous, A.; Schulz, B.; Hahn, G.; Bestmann, M.; Sharma, K.K. Neoproterozoic geodynamic in NW India—Evidence from Erinpura granites in the south Delhi Fold Belt. *Int. Geol. Rev.* **2022**, *64*, 1050–1080. [CrossRef]
58. Hine, R.; Williams, I.S.; Chappell, B.W.; White, A.J.R. Contrasts between I- and S-type granitoids of the Kosciusco Batholith. *J. Geol. Soc. Aust.* **1978**, *25*, 219–234. [CrossRef]
59. Laurent, O.; Martin, H.; Moyen, J.F.; Doucelance, R. The diversity and evolution of Late-Archean granitoids: Evidence for the onset of "modern-style" plate tectonics between 3.0 and 2.5 Ga. *Lithos* **2014**, *205*, 208–235. [CrossRef]
60. Johannes, W.; Holtz, F. *Petrogenesis and Experimental Petrology of Granitic Rocks*; Springer: Berlin/Heidelberg, Germany, 1996; p. 335.
61. Condie, K.C. Archean magmatism and crustal thickening. *Geol. Soc. Am. Bull.* **1973**, *84*, 2981–2992. [CrossRef]
62. Rudnick, R.L.; Gao, S. Composition of the continental crust. *Treatise Geochem.* **2003**, *3*, 1–64.
63. Li, S.; Chung, S.-L.; Wang, T.; Wilde, S.A.; Chu, M.F.; Pang, C.-J.; Guo, Q.Q. Water-fluxed crustal melting and petrogenesis of large-scale Early Cretaceous intercontinental granitoids in the southern Great Xing'an range, North China. *Geol. Soc. Am. Bull.* **2018**, *130*, 580–597. [CrossRef]
64. Watson, E.B.; Harrison, T.M. Zircon saturation revisited: Temperature and composition effects in a variety of crustal magma types. *Earth Planet. Sci. Lett.* **1983**, *64*, 295–304. [CrossRef]
65. Kelsey, D.E.; Clark, C.; Hand, M. Thermobarometric modelling of zircon and monazite growth in melt-bearing systems: Examples using model metapelitic and metapsammitic granulites. *J. Metamorph. Geol.* **2008**, *26*, 199–212. [CrossRef]
66. Boehnke, P.; Watson, E.B.; Trail, D.; Harrison, T.M.; Schmitt, A.K. Zircon saturation re-revisited. *Chem. Geol.* **2013**, *351*, 324–334. [CrossRef]
67. Miller, C.F.; McDowell, S.M.; Mapes, R.W. Hot and cold granites? Implications of zircon saturation temperatures and preservation of inheritance. *Geology* **2003**, *31*, 529–532. [CrossRef]
68. Yang, J.-H.; Peng, J.-T.; Zheng, Y.-F.; Hu, R.-Z.; Bi, X.-W.; Zhao, J.-H.; Huang, J.-C.; Zhang, B.-L. Petrogenesis of the Mesozoic Shuikoushan per-aluminous I-type granodioritic intrusion in Hunan Province, South China: Middle-lower crustal reworking in an extensional tectonic setting. *J. Asian Earth Sci.* **2016**, *123*, 224–242. [CrossRef]